Available online at www.sciencedirect.com
ScienceDirect
Journal of Sound and Vibration 310 (2008) 381–393
JOURNAL OF SOUND AND VIBRATION
www.elsevier.com/locate/jsvi

Analysis of motion stability of the flexible rotor-bearing system with two unbalanced disks

Xie Wenhui[a,*], Tang Yougang[a], Chen Yushu[b]

[a]Department of Naval Architecture and Ocean Engineering, School of Civil Engineering, Tianjin University, Tianjin 300072, PR China
[b]Department of Mechanics, School of Mechanical Engineering, Tianjin University, Tianjin 300072, PR China

Received 2 August 2007; received in revised form 2 August 2007; accepted 3 August 2007
Available online 24 September 2007

Abstract

The complicated dynamical behavior of a flexible rotor-bearing system is studied in this paper. The unsteady oil-film force model described by three functions is considered. The bifurcation and chaos behaviors were revealed by calculating the maximum Lyapunov exponent of the system. Two new phenomena were found in this system: first, the chaos with two attracting areas which cannot be distinguished from the stable period doubling motion on Poincarè section; second, for the flexible rotor system with two unbalanced disks, the response varies in a large extent when the phase angle between the eccentricities of disks is different. The experiments were also carried out. Comparison between experimental and calculated results shows that the significant use of the max Lyapunov exponent in revealing the bifurcation and chaos characteristics of the rotor-bearing system.

1. Introduction

A lot of researches have been done for Jeffcott rotor system that is a shaft attached with a disk, to reveal the phenomena of bifurcation and chaos. The bifurcations of periodic solution are usually analyzed by Floquet theory. For example using Floquet theory, Chen et al. obtained the stability boundaries of periodic motion in parameter plane of mass eccentricity-rotation speed [1–3]. Based on Cash model, Meng established the open–close crack model and studied the bifurcation and chaos of cracked rotor-bearing systems with nonlinear turbulent motion [4,5]. Ehrich described a typical nonlinear phenomenon of casing-rub, and studied the so-called "natural border frequency" near sub-harmonic and super-harmonic resonances [6]. Goldman and Muszyska presented a mathematical model of rubbing force and revealed the sub-harmonic response and chaos alternating along with the increase of rotation speed [7]. Chu studied rotor system in rub event, and analyzed the path of entering into and out the regime of chaos [8–10]. Quasi-periodic and chaotic behaviors of an unbalanced rigid rotor veering systems were found by Kim and Noah [11] and Abu-Mahfouz [12]. The response of an unbalanced rotor/bearings system with nonlinear suspension was investigated numerically by Chen and Yau [13]. Jump phenomena, sub-harmonic and quasiperiodic vibrations were found. Badgley and Booker [14] investigated the effects of residual unbalance on the cylindrical motion. The rotor was modeled by means of five independent coordinates, which are

*Corresponding author.
E-mail address: xiewh_td@163.com (X. Wenhui).

0022-460X/$ - see front matter © 2007 Elsevier Ltd. All rights reserved.
doi:10.1016/j.jsv.2007.08.001

the coordinates of the rotor mass center in plane orbits and the three Euler angles. For such rotors, Adiletta, Guido, and Rossi found some theoretical and experimental results for the cylindrical motion and pointed out the possible chaotic motions stemming from the nonlinear response of the bearings [15,16]. The Muszynska model [17–19] was introduced as a simple model of nonlinear fluid dynamic forces generated in bearings as well as in seals based on the results of a series of experiments. A parameter called the fluid average circumferential velocity ratio is used to describe the characteristic of the fluid motion as a whole. The fluid film radial stiffness, damping, and inertia effects are described by nonlinear functions of the rotor eccentricity ratio inside the bearing and seal. Adopting the Muszynska model, Ding et al. [20] investigated the Hopf bifurcation of a rotor/seal system. The level of unbalance on the bifurcation of synchronous whirl was discussed.

These researches result comprehensively illuminate the bifurcation and stability of motion of Jeffcott rotor/bearing system with single disk. Whereas the researches on the rotor system with multidisk are rather limited. Some procedures for balancing large multibearing rotors machines have been established [21]. A nonlinear mathematical model which includes the nonlinear oil bearings was employed for the on-site identification of unbalance change by Krodkiewski et al. [22]. Recently, the dynamics of a multibearing rotor attached with two disks are investigated experimentally by Ding and Leung. A phenomenon that the pre-existing non-synchronous whirl/whip resulted from the instability of one shaft can activate the onset of oil instability of its neighboring shaft is revealed [23].

In this paper, the bifurcation and chaos characteristics of a flexible rotor system with two unbalanced disks are investigated using the maximum Lyapunov exponent. The results show that the maximum Lyapunov exponent is a valid method in identifying the bifurcation and chaos characteristics for rotor-bearing system. Experimental result carried on a test rig supports partly the theoretical analysis.

2. Equation of motion

2.1. Analytical model

Fig. 1 shows the model of a flexible rotor system with two unbalanced disks. The mass of flexible shafts is concentrated to the disks and the ends, k_1, k_2 and k_3 denote the bending stiffness of three spans of shaft, respectively. O_2 and O_3 are geometrical center of the disks 2 and 3, O_1 and O_4 are center of left and right axle neck, respectively; c_2 and c_3 are the centers of masses of disks 2 and 3, bearings 1 and 4 are the journal bearings; Φ is the phase angle between the eccentricity of disks 2 and 3. x_i, y_i $i = 1, 2, 3, 4$ represent horizontal and vertical displacements.

2.2. Dynamical equation

The dynamical equations of the flexible rotor system are deduced as

$$\begin{cases} \ddot{Z}_1 = \omega_{11}^2(Z_2 - Z_1) + \dfrac{F_1}{m_1} - jg, \\ \ddot{Z}_2 = -\omega_{21}^2(Z_2 - Z_1) + \omega_{22}^2(Z_3 - Z_2) + e_2\Omega^2 e^{j\Omega t} - jg, \\ \ddot{Z}_3 = -\omega_{32}^2(Z_3 - Z_2) + \omega_{33}^2(Z_4 - Z_3) + e_3\Omega^2 e^{j(\Omega t + \Phi)} - jg, \\ \ddot{Z}_4 = -\omega_{43}^2(Z_4 - Z_3) + \dfrac{F_4}{m_4} - jg, \end{cases} \tag{1}$$

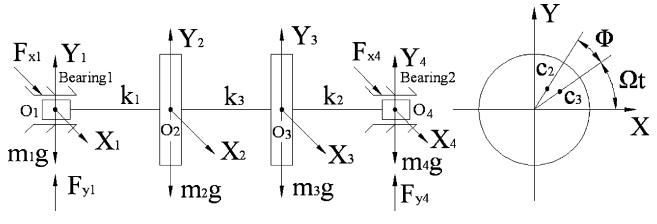

Fig. 1. Analytical model.

where $\omega_{lm}^2 = k_m/m_l$, $l = 1, 2, 3, 4$, $m = 1, 2, 3$; $Z_j = x_j + iy_j$, $j = 1, 2, 3, 4$. $m_k (k = 1, 2, 3, 4)$ represent the masses of the disks and necks; $e_q (q = 2, 3)$ are the eccentricities of the disks; $F_r = F_{xr} + jF_{yr}$, $r = 1, 4$, F_{x1}, F_{y1}, F_{x4}, F_{y4} are oil-film forces of bearing 1 and 4 in x-direction and y-direction, respectively [24], which are expressed as

$$\begin{bmatrix} F_{xr} \\ F_{yr} \end{bmatrix} = -C \begin{bmatrix} \dot{X}_r \\ \dot{Y}_r \end{bmatrix} - K \begin{bmatrix} X_r \\ Y_r \end{bmatrix}, \tag{2}$$

where

$$C = \begin{bmatrix} C_{11} & C_{12} \\ C_{21} & C_{22} \end{bmatrix}, \quad K = \frac{1}{2} \begin{bmatrix} -C_2 & C_3 \\ -C_3 & C_2 \end{bmatrix}, \quad C_{11} = C_1 \cos^2\phi_r + C_3 \sin^2\phi_r - 2C_2 \sin\phi_r \cos\phi_r, \quad C_{12} = C_{21},$$

$$C_{21} = C_2(\cos^2\phi_r - \sin^2\phi_r) + (C_1 - C_3)\sin\phi_r \cos\phi_r, \quad C_{22} = C_1 \sin^2\phi_r + C_3 \cos^2\phi_r + 2C_2 \sin\phi_r \cos\phi_r,$$

$$C_1 = \frac{4\varepsilon_r \dot{\varepsilon}_r A\left[3A^2 + (2 - 5\varepsilon_r^2)\varepsilon_r^2\left(\dot{\phi}_r - \frac{1}{2}\right)^2\right]}{(1 - \varepsilon_r^2)^2\left[A^2 - \varepsilon_r^4\left(\dot{\phi}_r - \frac{1}{2}\right)^2\right]^2} + \frac{2 + 4\varepsilon_r^2}{(1 - \varepsilon_r^2)^{5/2}}\Delta\phi_r, \quad C_2 = \frac{8A\varepsilon_r^4\left(\dot{\phi}_r - \frac{1}{2}\right)^3}{\left[A^2 - \varepsilon_r^4\left(\dot{\phi}_r - \frac{1}{2}\right)^2\right]^2},$$

$$C_3 = \frac{4\varepsilon_r \dot{\varepsilon}_r A\left[A^2 + (\varepsilon_r^2 - 2)\varepsilon_r^2\left(\dot{\phi}_r - \frac{1}{2}\right)^2\right]}{(1 - \varepsilon_r^2)\left[A^2 - \varepsilon_r^4\left(\dot{\phi}_r - \frac{1}{2}\right)^2\right]^2} + \frac{2}{(1 - \varepsilon_r^2)^{3/2}}\Delta\phi_r, \quad A = \sqrt{\dot{\varepsilon}_r + \left(\dot{\phi}_r - \frac{1}{2}\right)^2 \varepsilon_r^2},$$

$$\Delta\phi = \pi + 2\tan^{-1}\left(\frac{\varepsilon_r \dot{\varepsilon}_r}{A(1 - \varepsilon_r^2)^{1/2}}\right), \quad \dot{\phi}_r = \frac{x_r \dot{y}_r - y_r \dot{x}_r}{\sqrt{x_r^2 + y_r^2}}, \quad \dot{\varepsilon}_r = \frac{x_r \dot{x}_r + y_r \dot{y}_r}{\varepsilon_r}, \quad \varepsilon_r = \frac{\sqrt{x_r^2 + y_r^2}}{\delta}.$$

where, ϕ_r is the angular coordinate of the center of axle neck, x_r, y_r are rectangular coordinate of the center of axle neck, $r = 1, 4$, δ is the average clearance of the bearings.

Ω is the rotation speed of the rotor and g the gravity acceleration. Introducing the following non-dimensional variables:

$$\left.\begin{gathered} z_1 = \frac{Z_1}{\delta}; \quad z_1 = \frac{Z_2}{\delta}; \quad z_3 = \frac{Z_3}{\delta}; \quad z_4 = \frac{Z_4}{\delta}; \quad \tau = \Omega t \\ \bar{\omega}_{ij} = \frac{\omega_{ij}}{\Omega}, i, j = 1, 2, 3, 4; \quad \varsigma_2 = \frac{e_2}{\delta}; \quad \varsigma_3 = \frac{e_3}{\delta}; \quad \bar{g} = \frac{g}{\delta\Omega^2}; \quad f_i = \frac{F_i}{\delta\Omega^2}, i = 1, 4 \end{gathered}\right\}. \tag{3}$$

Eq. (1) can be rewritten in non-dimension form:

$$\begin{cases} z_1'' = \bar{\omega}_{11}^2(z_2 - z_1) + \dfrac{f_1}{m_1} - j\bar{g}, \\ z_2'' = -\bar{\omega}_{21}^2(z_2 - z_1) + \bar{\omega}_{22}^2(z_3 - z_2) + \varsigma_2 e^{j\Omega t} - j\bar{g}, \\ z_3'' = -\bar{\omega}_{32}^2(z_3 - z_2) + \bar{\omega}_{33}^2(z_4 - z_3) + \varsigma_3 e^{j(\tau + \Phi)} - j\bar{g}, \\ z_4'' = -\bar{\omega}_{43}^2(z_4 - z_3) + \dfrac{f_4}{m_4} - j\bar{g}, \end{cases} \tag{4}$$

where "′" represent the difference to "τ".

3. Calculation result

Let $m_1 = m_4 = 0.2\,\text{kg}$, $m_2 = m_3 = 1.1\,\text{kg}$, $k_1 = k_2 = 100{,}000\,\text{N/m}$, $k_3 = 400{,}000\,\text{N/m}$, $\delta = 250\,\mu\text{m}$; diameter and width of bearings are 25 mm and 16 mm; kinetic viscosity of lubricant $\mu = 0.05\,\text{Pa s}$. The maximum Lyapunov exponent (max-Le) and bifurcation diagrams in term of rotation speed are calculated by numerical method for different eccentricity and the phase angle of the unbalanced mass between disks 2 and 3, as shown in Table 1 for six cases.

Table 1
Parameters of eccentricities of masses

	Case 1	Case 2	Case 3	Case 4	Case 5	Case 6
e_2 (m)	0.000175	0.000225	0.0001	0.000125	0.0001	0.00025
e_3 (m)	0	0	0.0001	0.000125	0.0001	0.00025
Φ (deg)	0	0	30	30	150	150

Table 2
The relation between the motion behavior and the max-Le for the phase angle $|\Phi| \leqslant \pi/2$

Case 1	Rotation frequency	<32 Hz	[32–42] Hz	[42–58] Hz	(58–60.5) Hz	[60.5–63.5] Hz	<63.5 Hz
	Max-Le	<0	>0	<0	>0	<0	>0
	Stability of motion	Stable	Unstable	Stable	Unstable	Stable	Unstable
Case 2	Rotation frequency	<32 Hz	[32–46) Hz	[46–65] Hz	>65 Hz		
	Max-Le	<0	>0	<0	>0		
	Stability of motion	Stable	Unstable	Stable	Unstable		
Case 3	Rotation frequency	<32 Hz	[32–43.5] Hz	(43.5–58) Hz	[58–61) Hz	[61–64] Hz	<64 Hz
	Max-Le	<0	>0	<0	>0	<0	>0
	Stability of motion	Stable	Unstable	Stable	Unstable	Stable	Unstable
Case 4	Rotation frequency	<30 Hz	[30–46.5) Hz	[46.5–65] Hz	>65 Hz		
	Max-Le	<0	>0	<0	>0		
	Stability of motion	Stable	Unstable	Stable	Unstable		

Table 2 shows relations between the motion behavior and the max-Le of four cases with the phase angle $|\Phi| \leqslant \pi/2$. Figs. 2–5 are the max-Le and bifurcation diagram for cases 1, 2, 3, 4, respectively.

One finds that five kinds of system motion exist over rotation frequency of 10–100 Hz. They are the stable single period motion, the unstable primary resonance motion, the stable period doubling motion, the quasi-period or multiperiod motion, the chaos motion with one or two chaos attractant area, respectively. For case 1, the period doubling motion occurs within the rotation frequency from 60.5 to 63.5 Hz. When rotation frequency is a little higher than 63.5 Hz, the motion can reasonably be considered as the stable period doubling motion from the bifurcation diagram. But, in fact, it is the chaotic motion with two attracting area, because the max-Le is more than 0. For case 2, the period doubling bifurcation occurs when the rotation frequency is 58 Hz. The period doubling motion occurs within the rotation frequency from 58 to 65 Hz. When rotation frequency is a little higher than 65 Hz, the motion is the chaotic motion with two attracting area. For case 3, the period doubling motion occurs within the rotation s frequency from 61 to 64 Hz. When rotation frequency is a little higher than 64 Hz, the motion is the chaotic motion with two attracting area. For case 4, the period doubling bifurcation occurs when the rotation frequency is 58 Hz. The period doubling motion occurs within the rotation frequency from 58 to 65 Hz. When rotation frequency is a little higher than 65 Hz, the motion is the chaotic motion with two attracting area.

Table 3 shows relations between the motion behavior and the max-Le of two cases for the phase angle $\pi/2 < |\Phi| \leqslant \pi$. Figs. 6 and 7 are the max-Le and bifurcation diagram for cases 5, 6, respectively.

One finds that the four kinds of system motion exist over rotation frequency of 10–100 Hz for the phase angle $\pi/2 < |\Phi| \leqslant \pi$. They are the stable single period motion, the quasi-period or multiperiod motion, the first chaos motion, the chaos motion with two chaos attractant areas, respectively. The period doubling motion does not occur.

Fig. 8 shows the bifurcations of the system with different unbalance values. They show that the response with same eccentricities is quite different for $\Phi = 90^\circ$ and 180°.

From above calculation results, we can conclude that for $|\Phi| \leqslant \pi/2$ (see Figs. 2–5 and 8(a), 8(b)), the period doubling bifurcation and the quasi-period or the multiperiod bifurcation will occur, and the motion will lost its stability and gets into chaos along with increase of the rotation speed; The unstable primary resonance will increase along with increasing the eccentricity of the rotor; And frequency range of 1/2 sub-harmonic motion can be obtained. Moreover, comparing Figs. 2, 4, and 8(a) with Figs. 3, 5, and 8(b), respectively, one find that

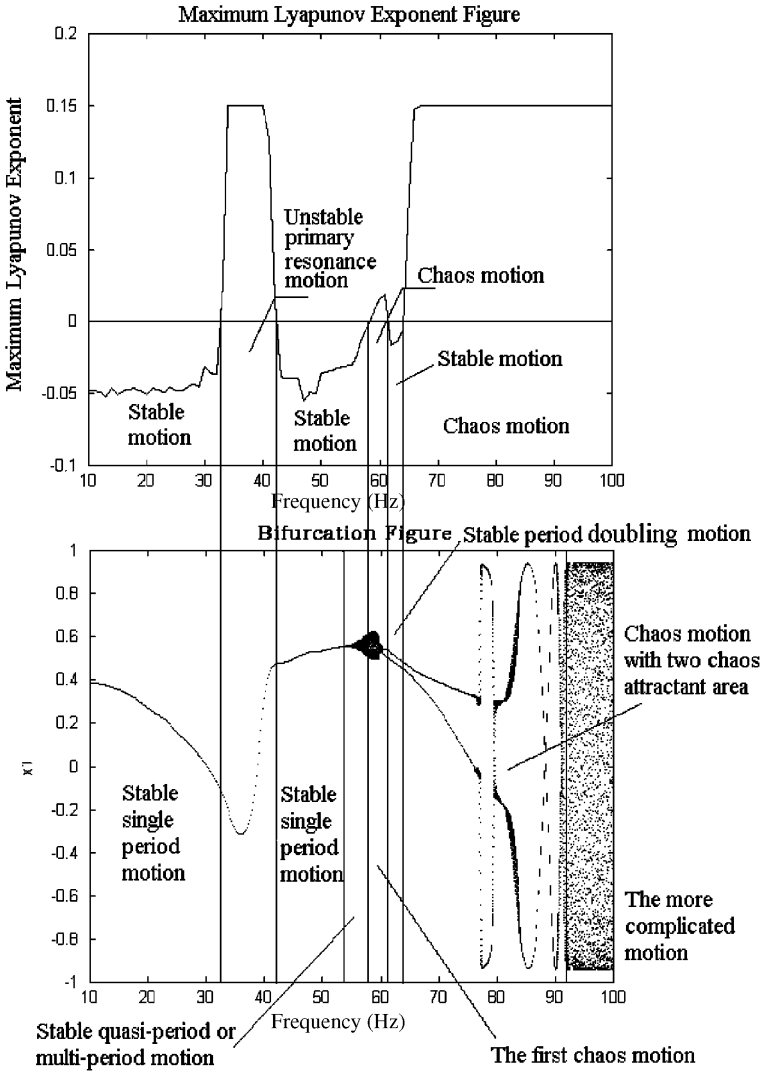

Fig. 2. The max-Le and bifurcation diagram for case 1.

the jump phenomenon increase around the primary natural frequency (about 40 Hz) along with the eccentricity increasing. For $\pi/2<|\Phi|\leqslant\pi$ (see Figs. 6, 7, and 8(c), (d)), the quasi-period bifurcation or the multiperiod bifurcation will occur, and the motion lost stability and get into chaos along with the rotation frequency increasing. One cannot find the distinctly amplitude variety around the primary natural frequency (about 40 Hz) for the rotor. Further, the stable 1/2 sub-harmonic motion will not occur in this case. For $|\Phi|\leqslant\pi/2$ or $\pi/2<|\Phi|\leqslant\pi$, the chaos motion with two attractant area will occur at the high rotation speed in this rotor system. From conclusions above, the system response is different when the phase angle of the eccentricity of disks is $|\Phi|\leqslant\pi/2$ or $\pi/2<|\Phi|\leqslant\pi$. So utilizing this characteristic one can estimated the eccentricity of rotor system.

4. Experimental results

The experimental studies are carried out on the test rotor rig as shown in Fig. 9. The lengths $L_1 = L_2 = L_3 = 15.5$ cm, diameter of the shaft is 12 mm, masses of two disks are 0.99 kg, respectively. Added mass is used to change the imbalance level of disks.

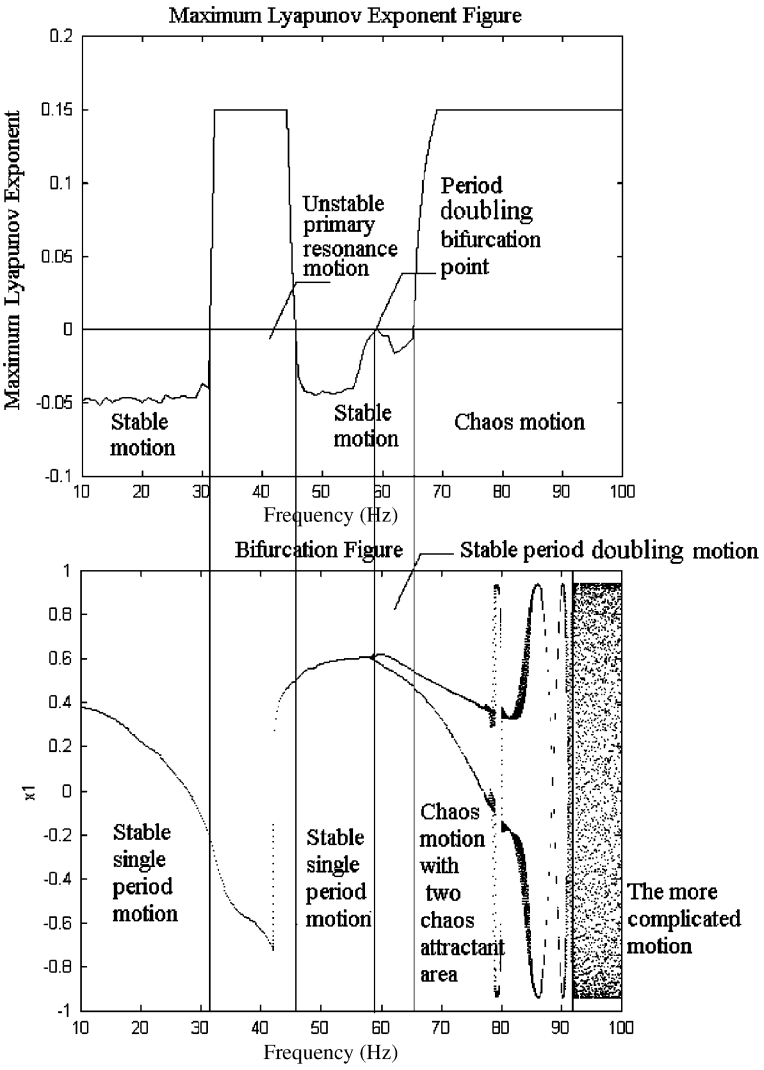

Fig. 3. The max-Le and bifurcation diagram for case 2.

4.1. Experiment 1: without added mass

The test rig consists of shaft, disks, bearing, motor, and restricted plane board. Owing to the axisymmetric mass arrangement, Fig. 10 presents spectrum cascade and selected orbits of journal 1 only. The spectrum cascade indicates that the rotating speed grows quite fast in passing through the critical speed at 28.3 Hz to avoid severe rubs between the shaft and the restricted plane board and the occurrence of rub-induced backward whirl. Such a backward whirl can lead the rotor to fail when passing the critical speed [25]. The rotating speed can be controlled to increase slowly and steadily after passing the critical speed, especially when operating in oil whirl regime. The transition from synchronous whirl to non-synchronous whirl, known also as "oil whirl" or "instability," is encountered at the threshold speed 50.9 Hz ($t = 58.2$ s). Besides the pre-existing component of the rotating speed F_{rot}, the whirling frequency F_{whirl} component appears also in the spectrum after the threshold speed is exceeded. The whirling frequency F_{whirl} at the onset of instability F_{whirl} is found to be 25.4 Hz, which is nearly 3 Hz lower than the critical speed and equals to half of F_{rot}. So the instability results in a period-doubling bifurcation. As the rotating speed increases further, F_{whirl} increases simultaneously and keeps the 1:2 ratio with F_{rot}. The whirl orbit of journal 1 at $F_{\text{rot}} = 52$ Hz shows clearly a period 2 motion, that is a large circle and a small circle appear alternately as time goes on.

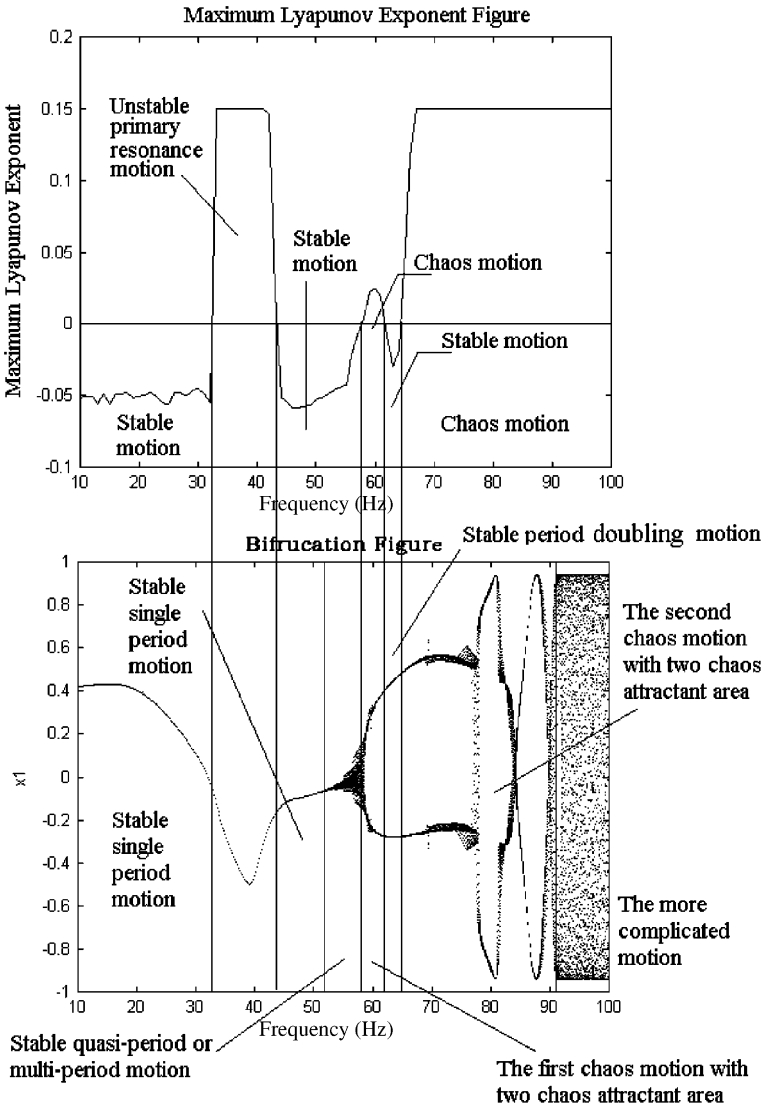

Fig. 4. The max-Le and bifurcation diagram for case 3.

With increasing F_{rot} and F_{whirl}, their magnitudes gradually decrease and grow, respectively. As F_{whirl} is approaching the critical frequency 28.3 Hz, a resonance known as "oil whip" in engineering happens at $F_{\text{rot}} = 54.35$ Hz. During the oil whip regime, the whirl orbit grows very rapidly. The spectrum is already dominated by the F_{whirl} component and the smaller circles have disappeared from the whirl orbit as manifested in the whirl orbit at $F_{\text{rot}} = 55.2$ Hz. The rotating speed of the rotor can hardly be increased further hereafter because most energy provided by the power-limited motor is transferred from the rotation to maintain the non-synchronous (half-frequency) whirl. Staying in the oil whip regime for a long time is damaging to the test rig as severe vibration may cause partial rubs between the shaft and the restricted plane board. So the rotating speed should be decreased in time. Careful check shows that during the speed-down, the rotor transits from the non-synchronous whirl to synchronous whirl at 47.8 Hz, which is 3.1 Hz lower than the threshold speed 50.9 Hz during speed-up. The difference between the two transition speeds proves a commonly known delay phenomenon [26].

From the numerical simulation results when the phase angle $|\Phi| \leqslant \pi/2$, the primary natural frequency of rotor-bearing system is about 40 Hz. The period double motion occurs when the rotation frequency F_{rot} is

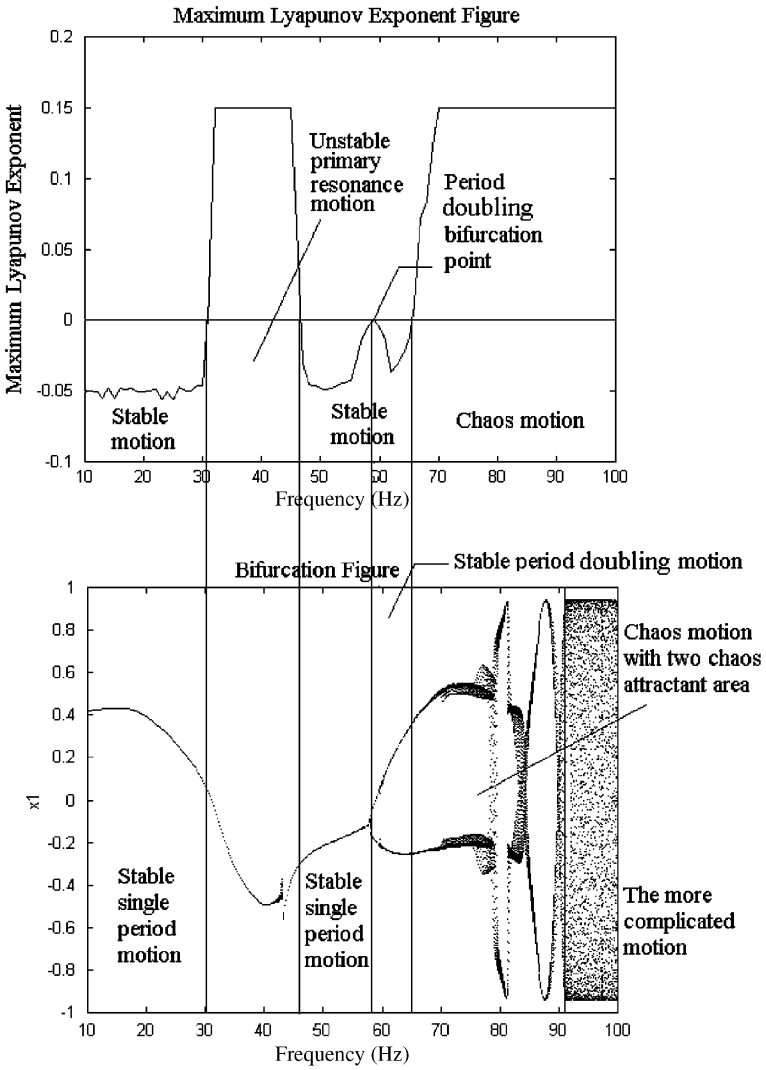

Fig. 5. The max-Le and bifurcation diagram for case 4.

Table 3
The relation between the motion behavior and the max-Le for the phase angle $\pi/2 < |\Phi| \leqslant \pi$

Case 5	Rotation speed	<60.5 Hz	$\leqslant 60.5$ Hz
	Max-Le	<0	>0
	Stability of motion	Stable	Unstable
Case 6	Rotation speed	<62.5 Hz	$\leqslant 62.5$ Hz
	Max-Le	<0	>0
	Stability of motion	Stable	Unstable

about 58 Hz. With increasing F_{rot}, the chaos motion with two chaos attractant areas occurs when the rotation frequency F_{rot} is about 65 Hz. When the period doubling motion or the chaos motion with two chaos attractant areas occurs, F_{rot} and F_{whirl} frequency components must be predominant in response. As F_{whirl} is approaching the critical frequency 40 Hz, the magnitude of $x1$ grows very rapidly at about $F_{\text{rot}} = 80$ Hz. F_{whirl} frequency components must be predominant in response. So a resonance known as "oil whip" in engineering

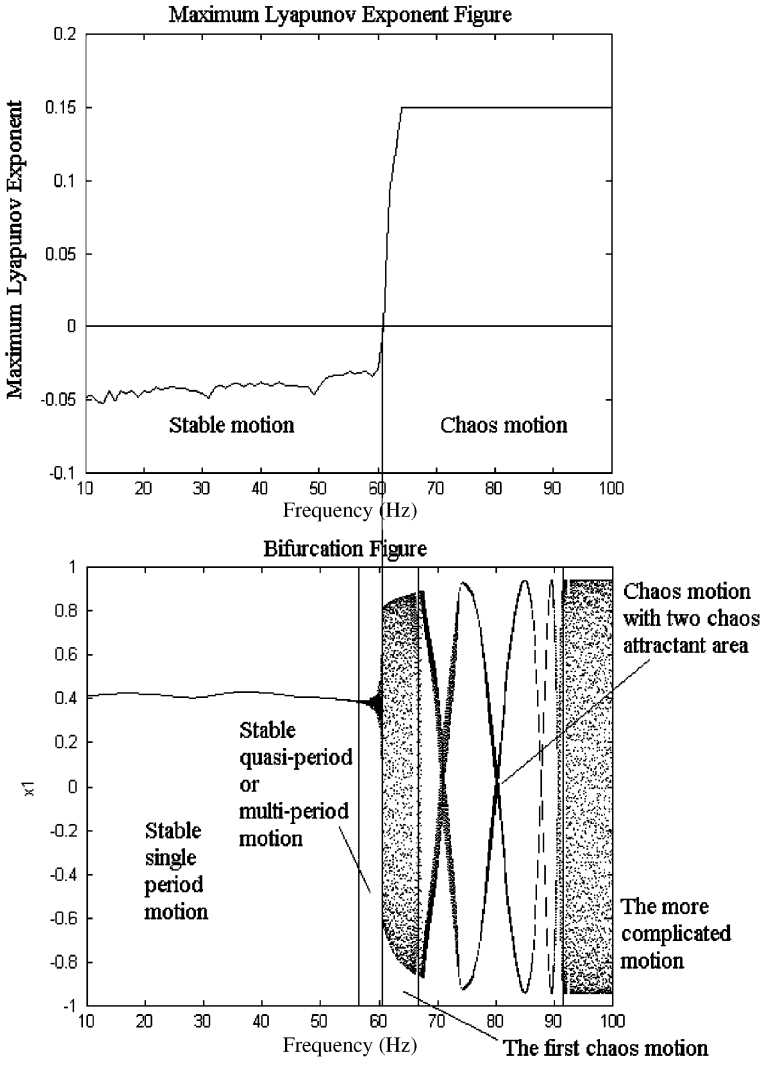

Fig. 6. The max-Le and bifurcation diagram for case 5.

happens. All these show that the numerical simulation results for $|\Phi| \leqslant \pi/2$ and experimental results for the perfectly balanced disk are qualitatively equivalent.

4.2. Experiment 2: using added mass

The spectrum cascades of horizontal motions of the imbalanced rotor, by attaching a little added mass to the disk 2, are presented in Fig. 11. In order to avoid violent vibration the rotating speed grows quite fast in passing through the critical speed at 29.3 Hz. But the vibration amplitude did not distinctly increase in passing through the critical speed at F_{whirl} 29.3 Hz. This shows the influence of the different imbalance. Moreover, when operating in oil whirl regime, the whirl orbit of journal 1 do not shows clearly a period 2 motion, that is only a large circle as time goes on. These show that F_{whirl} frequency components are predominant. Other dynamics phenomena are basically same with that no added mass.

From the numerical simulation results when the phase angle $\pi/2 < |\Phi| \leqslant \pi$, the vibration magnitude of $x1$ do not remarkably increase at the primary natural frequency about 40 Hz. While the vibration amplitude did not also distinctly increase at the primary natural frequency in the experimental results. The period doubling

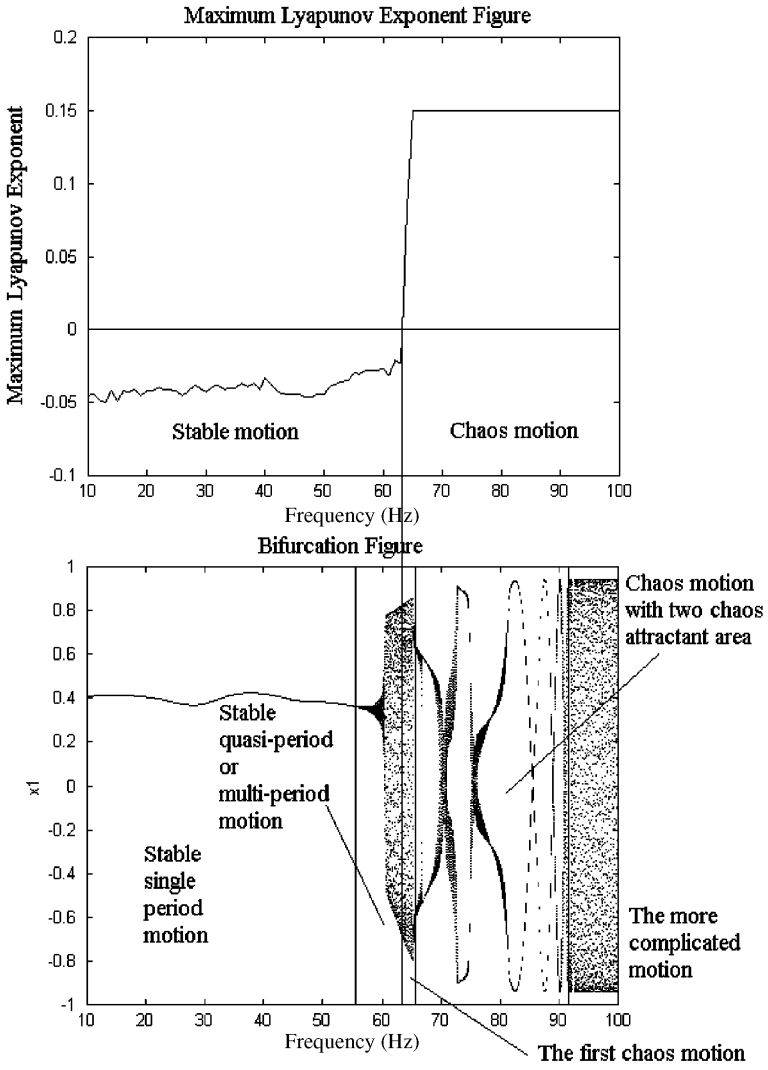

Fig. 7. The max-Le and bifurcation diagram for case 6.

motion do not occurs, but with increasing F_{rot}, the chaos motion with two chaos attractant area occurs when the rotation frequency F_{rot} is about between 67 and 92 Hz, and the magnitude of $x1$ increases or decreases very rapidly within [67 and 92 Hz]. So the oil whip in engineering happens. F_{whirl} frequency components must be predominant in this time. From the experimental results, the whirl orbit of journal 1 at $F_{rot} = 52.4$ and 55.3 Hz shows that is only a large circle as time goes on, so F_{whirl} frequency components is also predominant in this time. All these show that the numerical simulation results for $\pi/2 < |\Phi| \leqslant \pi$ and experimental results for the disk using added mass are similar.

5. Conclusion

Investigation of a rotor-bearing system with two disks shows that the max Lyapunov exponent is valid method in identifying the bifurcation and chaos character of the flexible rotor system supported on lubricated bearing. The chaos with two attractant area is found which cannot be distinguished from the stable period double motion using Poincarè section; Second, five types motion patterns including the stable single period motion, the unstable primary resonance motion, the stable quasi-period or multiperiod motion, the stable doubling period motion and the chaos motion with one or two attractant area are obtained. Third, for the

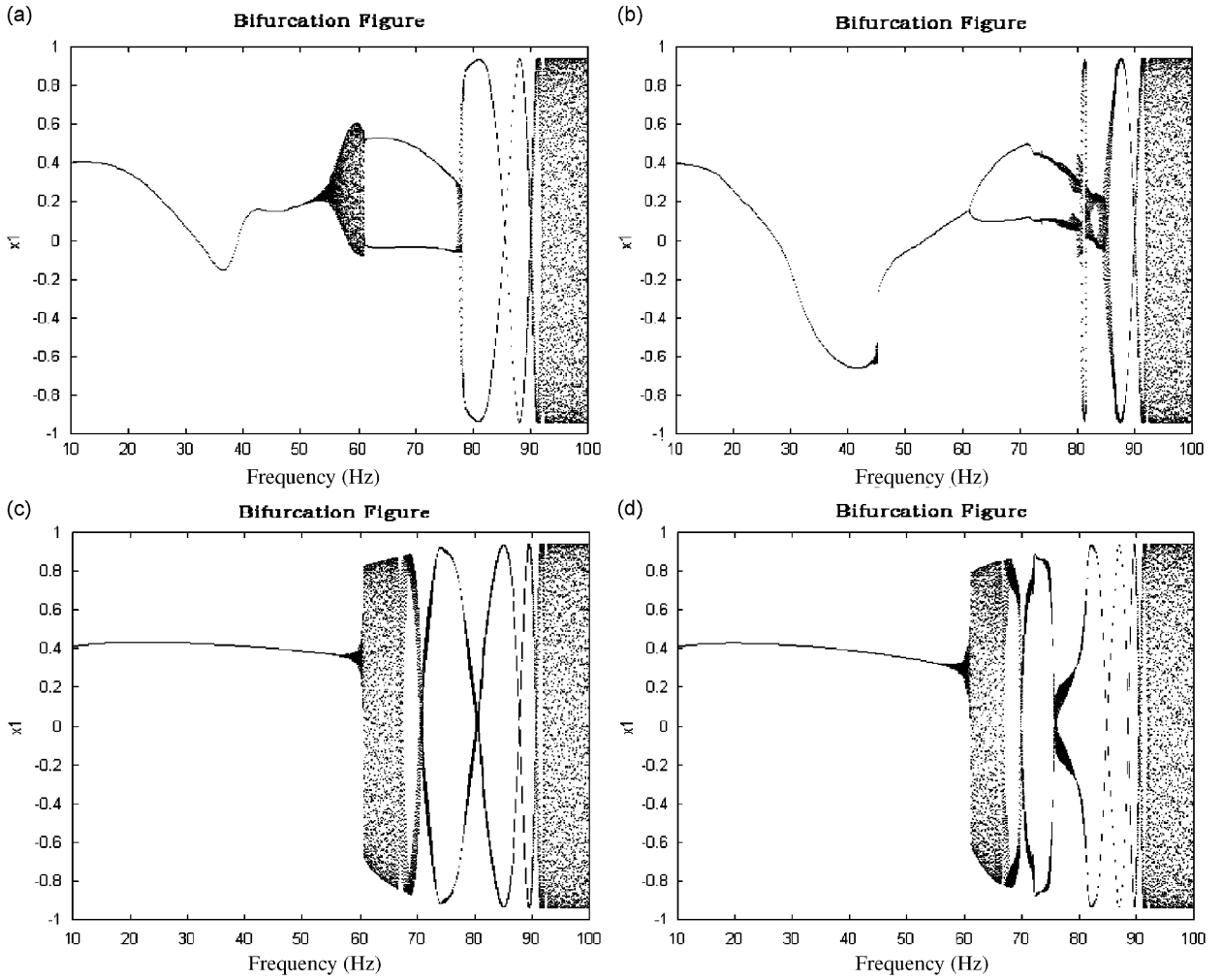

Fig. 8. Bifurcations with different unbalance values: (a) $e_2 = 0.0001$, $e_3 = 0.0001$, $\Phi = 90^\circ$, (b) $e_2 = 0.0002$, $e_3 = 0.0002$, $\Phi = 90^\circ$, (c) $e_2 = 0.0001$, $e_3 = 0.0001$, $\Phi = 180^\circ$ and (d) $e_2 = 0.0002$, $e_3 = 0.0002$, $\Phi = 180^\circ$.

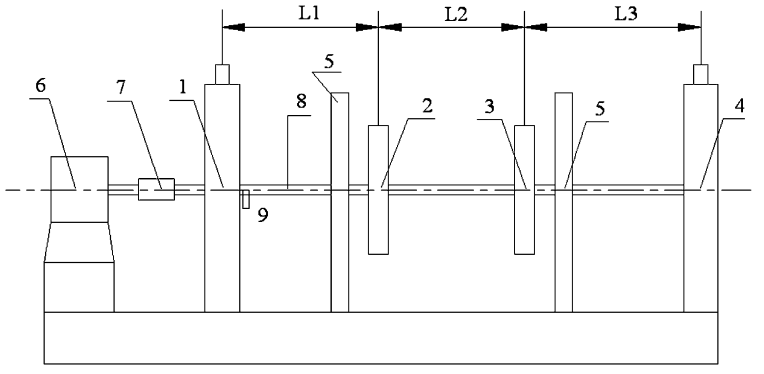

1,2-Sliding Bearing 3,4-Disk 5-Restricted Plane Board 6-Motor

7-Flexible Joint 8-Shaft 9-Transducer

Fig. 9. The experiment model of the rotor system.

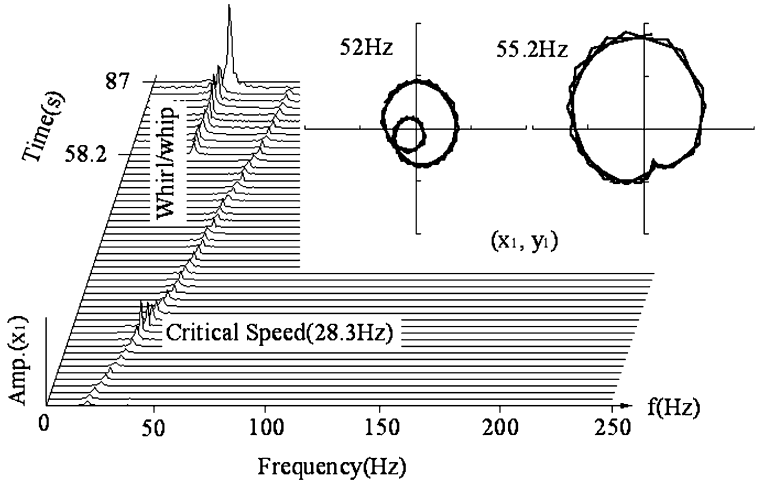

Fig. 10. Experimental result: spectrum cascade and selected orbits (x_1, y_1).

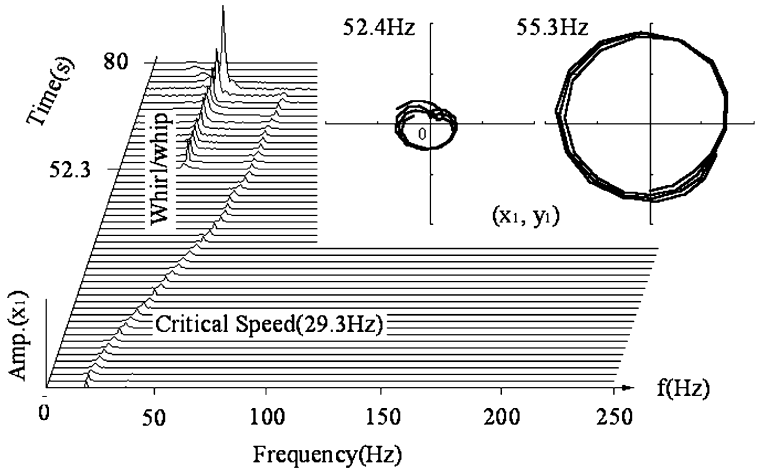

Fig. 11. Experimental result: spectrum cascade and selected orbits (x_1, y_1).

flexible rotor system with two unbalanced disks, the system response is very different when the phase angle of the eccentricity of disks is within $[0, \pi/2]$ and within $[\pi/2, \pi]$. So utilizing this characteristic one can estimate the eccentricity of rotating machinery in the practice.

Acknowledgment

The revision of this paper is supported by Professor Q. Ding. Hereon, we would like to thank for his previous works and his assistance.

References

[1] Chen Yushu, Meng Quan, Bifurcations of a nonlinear rotor-bearing system, *Journal of Vibration Engineering* 9 (3) (1996) 266–275 (in Chinese).

[2] Chen Yushu, Ding Qian, Meng Quan, Analysis of the instability of low frequency vibration of rotor system, *Journal of Applied Mechanics* 15 (1) (1998) 113–117 (in Chinese).

[3] Meng Quan, Chen Yushu, A study on the global bifurcations of nonlinear rotor-bearing system for 1/2 sub-harmonic resonance, *Journal of Nonlinear Dynamics* 33 (2) (1996) 89–197 (in Chinese).
[4] Meng Guang, The nonlinear influence of whirl speed on the stability and response of a cracked rotor, *Journal of Machine Vibration* 4 (1992) 216–230 (in Chinese).
[5] Zheng Jibing, Meng Guang, The nonlinear influences of whirl speed on bifurcation and chaos of a cracked rotor, *Journal of Vibration Engineering* 10 (2) (1997) 190–197 (in Chinese).
[6] F.F. Ehrich, Spontaneous side banding in high speed rotor dynamics, *Journal of Vibration, Acoustics, Stress, Reliability in Design—Transactions of the ASME* 114 (1992) 418–505.
[7] P. Goldman, A. Muszynska, A chaotic behavior of rotor/stator with rubs, *Journal of Engineering for Gas Turbines and Power—Transactions of the ASME* 116 (1994) 692–701.
[8] F.L. Chu, T. Yun, Stability of rotor casing-rub, *Journal of Tsinghua University (Science and Technology)* 40 (4) (2000) 119–123 (in Chinese).
[9] F.L. Chu, F. Guan Ping, et al., Interval happening chaos of casing-rub rotor system, *Journal of Aerospace Power* 11 (3) (1996) 261–264.
[10] F.L. Chu, Z. Zhensong, Chaos character of casing-rub rotor system, *Journal of Tsinghua University (Science and Technology)* 36 (7) (1996) 52–57 (in Chinese).
[11] Y.B. Kim, S.T. Noah, Quasi-periodic response and stability analysis for a nonlinear Jeffcott rotor, *Journal of Sound and Vibration* 190 (2) (1996) 239–253.
[12] I.A. Abu-Mahfouz, Routes to Chaos in Rotor Dynamics, PhD Thesis, Case Western Reserve University, Cleveland, 1993.
[13] C.K. Chen, H.T. Yau, Bifurcation in a flexible rotor supported by short journal bearings with nonlinear suspension, *Journal of Vibration and Control* 7 (5) (2001) 653–673.
[14] R.H. Badgley, J.F. Booker, Rigid-body rotor dynamics: dynamic unbalance and lubricant temperature changes, *Journal of the Lubrication Technology—Transactions of the ASME* 92 (1970) 415–424.
[15] G. Adiletta, A.R. Guido, C. Rossi, Nonlinear dynamics of a rigid unbalanced rotor in journal bearings. 1. Theoretical analysis, *Nonlinear Dynamics* 14 (1) (1997) 57–87.
[16] G. Adiletta, A.R. Guido, C. Rossi, Nonlinear dynamics of a rigid unbalanced rotor in journal bearings. 2. Experimental analysis, *Nonlinear Dynamics* 14 (2) (1997) 157–189.
[17] A. Muszynska, Improvements in lightly loaded rotor/bearing and rotor/seal models, *Journal of Vibration Acoustics—Transactions of the ASME* 110 (2) (1988) 129–136.
[18] A. Muszynska, D.E. Bently, Frequency-swept rotating input perturbation techniques and identification of the fluid force models in rotor/bearing/seal systems and fluid handling machines, *Journal of Sound and Vibration* 143 (1) (1990) 103–124.
[19] A. Muszynska, D.E. Bently, Anti-swirl arrangements prevent rotor/seal instability, *Journal of Vibration Acoustics—Transactions of ASME* 111 (2) (1989) 156–162.
[20] Q. Ding, J.E. Cooper, A.Y.T. Leung, Hopf bifurcation analysis of a rotor/seal system, *Journal of Sound and Vibration* 252 (5) (2002) 817–833.
[21] J. Ding, Computation of multi-plane imbalance for a multi-bearing rotor system, *Journal of Sound and Vibration* 205 (3) (1997) 364–371.
[22] J.M. Krodkiewski, J. Ding, N. Zhang, Identification of unbalance change using a non-linear mathematical model for multi-bearing rotor systems, *Journal of Sound and Vibration* 169 (5) (1994) 685–698.
[23] Q. Ding, A.Y.T. Leung, Experimental study on nonlinear dynamic behaviours of a multi-bearing flexible rotor system, *Journal of Vibration and Acoustics—Transactions of the ASME* 127 (4) (2005) 408–415.
[24] X. Xiaofeng, Z. Wen, Bifurcation and chaos of rigid unbalance rotor in short bearings under an unsteady oil-film force model, *Journal of Vibration Engineering* 13 (2) (2000) 247–253 (in Chinese).
[25] Q. Ding, Y.S. Chen, Non-stationary whirl and instability of a shaft/casing system with rubs, *Journal of Vibration and Control* 7 (3) (2001) 327–338.
[26] Q. Ding, A.Y.T. Leung, Non-stationary processes of rotor/bearing system in bifurcation, *Journal of Sound and Vibration* 268 (1) (2003) 33–48.